

# Programmable Delivery of Fluoxetine via Wearable Bioelectronics for Wound Healing In Vivo

Houpu Li, Hsin-ya Yang, Narges Aseffeyzabadi, Prabhat Baniya, Andrea Medina Lopez, Anthony Gallegos, Kan Zhu, Tiffany Nguyen, Cristian Hernandez, Ksenia Zlobina, Cynthia Recendez, Hao-Chieh Hsieh, Maryam Tebyani, Héctor Carrión, John Selberg, Le Luo, Moyasar A. Alhamo, Alexie Barbee, Jonathan Orozco, Cathleen Hsieh, Athena M. Soulika, Michael Levin, Narges Norouzi, Marcella Gomez, Min Zhao, Mircea Teodorescu, Roslyn Rivkah Isseroff,\* and Marco Rolandi\*

The ability to deliver drugs with precise dosages at specific time points can significantly improve disease treatment while reducing side effects. Drug encapsulation for gradual delivery has opened the doors for a superior treatment regimen. To expand on this ability, programming bioelectronic devices to deliver small molecules enables ad-hoc personalized therapeutic profiles that are more complex than gradual release. Here, a wearable bioelectronic device with an integrated electrophoretic ion pump that affords on-demand drug delivery with precise dose control is introduced. Delivery of fluoxetine to wounds in mice result in a 27.2% decrease in the macrophage ratio (M1/M2) and a 39.9% increase in re-epithelialization, indicating a shorter inflammatory phase and faster overall healing. Programmable drug delivery using wearable bioelectronics in wounds introduces a broadly applicable strategy for the long-term delivery of a prescribed treatment regimen with minimal external intervention.

## 1. Introduction

The ability to tailor the therapeutic levels of drugs over time to the dynamic evolution of our physiology improves treatment effectiveness and leads to better clinical outcomes.<sup>[1]</sup> Research in drug delivery has developed materials and chemical strategies for passively and actively controlled release.<sup>[2]</sup> Merging this active control strategy for tunable drug delivery with programmable electronic devices can open the doors to personalized and more effective treatment regimens.<sup>[3]</sup> Bioelectronic devices are capable of delivering on-demand physiological-active ions,<sup>[4]</sup> small molecules,<sup>[3b,5]</sup> and electric fields as treatments.<sup>[6]</sup> This ability is

H. Li, N. Aseffeyzabadi, P. Baniya, T. Nguyen, C. Hernandez, H.-C. Hsieh, M. Tebyani, J. Selberg, L. Luo, A. Barbee, J. Orozco, M. Teodorescu, M. Rolandi

Department of Electrical and Computer Engineering  
University of California Santa Cruz  
Santa Cruz, CA 95064, USA

E-mail: [mrolandi@ucsc.edu](mailto:mrolandi@ucsc.edu)

H.-ya Yang, A. M. Lopez, A. Gallegos, M. A. Alhamo, A. M. Soulika, R. R. Isseroff

Department of Dermatology  
School of Medicine  
University of California Davis  
Davis, CA 95616, USA

E-mail: [risseroff@ucdavis.edu](mailto:risseroff@ucdavis.edu)

K. Zhu, C. Recendez, M. Zhao  
Department of Ophthalmology

School of Medicine  
University of California Davis  
Davis, CA 95616, USA

K. Zlobina, M. Gomez  
Department of Applied Mathematics  
University of California Santa Cruz  
Santa Cruz, CA 95064, USA

H. Carrión, N. Norouzi  
Department of Computer Science and Engineering  
University of California Santa Cruz  
Santa Cruz, CA 95064, USA

H.-C. Hsieh, C. Hsieh  
Department of Chemistry and Biochemistry  
University of California Santa Cruz  
Santa Cruz, CA 95064, USA

A. M. Soulika  
Pediatric Regenerative Medicine  
Shriners Hospitals for Children  
Sacramento, CA 95817, USA

M. Levin  
Department of Biology  
Tufts University  
Medford, MA 02155, USA

 The ORCID identification number(s) for the author(s) of this article can be found under <https://doi.org/10.1002/admt.202301115>

© 2024 The Authors. Advanced Materials Technologies published by Wiley-VCH GmbH. This is an open access article under the terms of the Creative Commons Attribution-NonCommercial-NoDerivs License, which permits use and distribution in any medium, provided the original work is properly cited, the use is non-commercial and no modifications or adaptations are made.

DOI: [10.1002/admt.202301115](https://doi.org/10.1002/admt.202301115)

particularly important when applied to rapidly changing environments, such as the one found in wounds.<sup>[7]</sup> Wound healing usually involves four overlapping phases: hemostasis, inflammation, proliferation, and remodeling.<sup>[8]</sup> A delay or disruption in one of these phases can lead to wound chronicity, scarring, infection, sepsis, and even death.<sup>[9]</sup> To facilitate wound healing, wearable bioelectronics have employed external stimuli, such as electric fields<sup>[10]</sup> and biochemicals.<sup>[11]</sup> To expand on these treatments, here we have developed a programmable bioelectronic device capable of delivering the drug fluoxetine (FLX), a selective serotonin reuptake inhibitor (SSRI) commonly used as an antidepressant agent, with the capacity to reduce inflammation<sup>[12]</sup> to accelerate healing in a mouse wound model (Figure 1). Prior studies have demonstrated that both systemic and topical administration of fluoxetine improves wound healing in both diabetic and non-diabetic rodent skin<sup>[13]</sup> as well as decreases wound pathogen growth, biofilm formation, and the dissemination of infection in rodents.<sup>[14]</sup>

## 2. Results and Discussion

The wearable bioelectronic device consists of two modules (Figure 1): an ion pump drug delivery module and a battery-powered controller module (Figure 1B). The controller module is responsible for translating a pre-programmed delivery profile into a sequence of voltage signals (Figure 1C), which activate the ion pump to deliver fluoxetine to the wound (Figure 1D). The ion pump drug delivery module consists of two reservoirs containing a fluoxetine solution. These reservoirs are connected to the wound bed through two glass capillaries filled with an ion-selective hydrogel. (Figure 2A). The module is made of polydimethylsiloxane (PDMS) using a casting process (see Experimental Section, Figure S1, Supporting Information). Two silver/silver chloride (Ag/AgCl) electrodes (a working electrode on the left and a counter electrode on the right) connect the reservoirs to the voltage source on the control module that drives the delivery of fluoxetine using  $V_{FLX}$ . To allow the delivery of fluoxetine, the solution in the reservoirs is acidic 0.01 M fluoxetine hydrochloride (FLX-HCl) tuned to pH 6, making fluoxetine positively charged (FLX $^+$ ) due to protonation (Figure S2, Supporting Information). When  $V_{FLX}$  is positive, FLX $^+$  molecules are pushed from the reservoir (on top part of Figure 2A) into the wound bed via the ion-selective hydrogel acting as an ion exchange membrane that blocks negatively charged anions entering the reservoirs from the wound bed. To maintain charge neutrality, we presume that physiological cations exit the wound bed through the ion-selective hydrogel on the right and enter the other reservoir that houses the counter electrode. These physiological cations also act as the charge carriers in the wound bed, completing the circuit. The difference in concentration between the physiological cations ( $\approx 150$  mM)<sup>[15]</sup> and fluoxetine ( $<0.3$  mM) in the wound bed ensures that most, if not all, of the

fluoxetine delivered to the wound bed does not escape into the reservoir containing the counter electrode.

Continuous delivery of FLX $^+$  occurs due to two opposite electrochemical reactions at the working and counter electrodes that maintain charge balance throughout the system (Figure 2B). In the reservoir containing the working electrode or anode (Figure 2B, top), the protonated FLX $^+$  is in FLX $^+$ -Cl $^-$  form to maintain charge neutrality. With  $V_{FLX} = 1\text{--}3$  V, an electron leaves the surface of the Ag, creating Ag $^+$ , which in turn reacts with the Cl $^-$  of the FLX-HCl to form AgCl. This reaction leaves the positively charged FLX $^+$  free to follow the electric field through the ion-selective hydrogel into the wound bed. To close the circuit, the opposite reaction occurs at the counter electrode (Figure 2B, bottom), where an electron from the leads creates Cl $^-$  that pairs with one of the physiological cations (such as Na $^+$  or K $^+$ ) that entered the reservoir from the wound bed, leaving an Ag surface and a salt.

The ion pump module comprises four reservoirs and four pins in contact with the Ag/AgCl electrodes (Figure 2C). The pins also provide mechanical coupling between the two modules (Figure 2D). Two reservoirs deliver FLX $^+$  into the wound bed, while the remaining two house the reference/counter electrodes. COMSOL simulations result in a uniform distribution of FLX $^+$  on the wound for this delivery strategy (Figure S3, Supporting Information). On top of the ion pump module (Figure 2D,E), the control module contains microcontrollers, analog-to-digital converters, and a battery that powers the wearable device so that it can function wirelessly between dressing changes. The control electronics translate the delivery regimen stored in memory into  $V_{FLX}$  pulses (Figure 2F).

We tested the ion pump delivery module in a well plate with saline solution and substituted the control module with a potentiostat (Figure 2G). We measured the current in the circuit ( $I_{FLX}$ ) while  $V_{FLX}$  underwent a series of pulses ranging from 0–2 V with a duration of 200 ms each. As expected, since the delivery circuit comprises all linear elements,  $I_{FLX}$  increases linearly with  $V_{FLX}$ . According to our description of the delivery mechanism (Figure 2A,B),  $I_{FLX}$  is proportional to the number of FLX $^+$  molecules delivered to the wound bed. To characterize the working efficiency of the ion pump, we measured the amount of FLX $^+$  delivered after a specific number of pulses into the saline solution by HPLC-MS (refer to SI text, Figures S4 and S5, Table S1, Supporting Information). The HPLC-MS results showed that the delivery efficiency ( $\eta$ ) was  $20 \pm 4\%$ , meaning that we delivered one FLX $^+$  molecule for every five electrons going through the circuit. This efficiency is in line with other ion pumps, and FLX $^+$  is likely to face competition from H $^+$ .<sup>[16]</sup> Calculating  $\eta$  allows us to infer the FLX $^+$  dose from measuring  $I_{FLX}$  during delivery.

We then proceeded to test the efficacy of the wearable bioelectronic device *in vivo* on a mouse wound model (Figure 3). We created a 6 mm punch wound held open by a silicone splint ring to minimize wound contraction (Figure 3A). Wound contraction is a major wound-healing process in mice but not humans. It confounds the histological analysis of the wound response to therapy, particularly re-epithelialization.<sup>[13b,14]</sup> The lightweight device (2.5 g) affixed with Tegaderm allowed the mouse to move around its cage without interference (Figure 3B). We programmed the delivery of FLX $^+$  for three days, six hours per day (Figure 3C) for a desired dose of 100 nMol of fluoxetine each day. This FLX $^+$

R. R. Isseroff  
Dermatology Section  
VA Northern California Health Care System  
Mather, CA 95655, USA

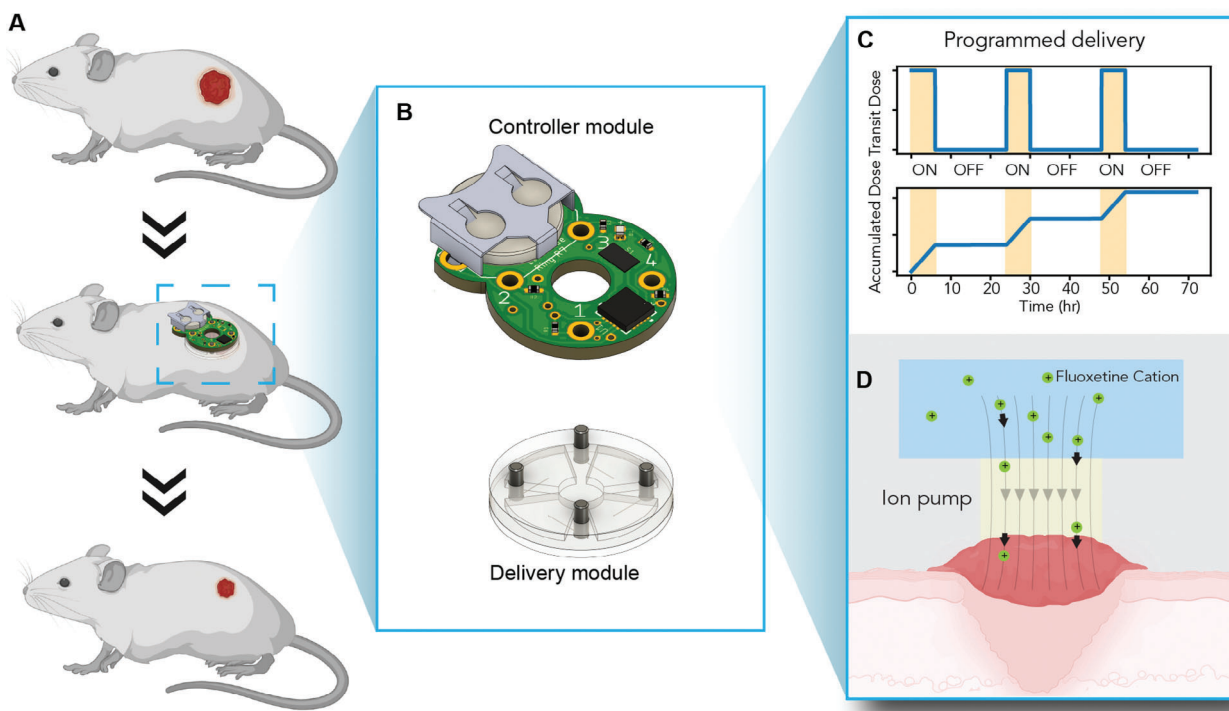


**Figure 1.** Depicts the wearable bioelectronic device designed for programmable drug delivery. A) A schematic of the wearable bioelectronic device applied to a mouse model. B) A CAD design of the wearable bioelectronic device, consisting of a battery-powered PCB controller module (top) and an ion pump made from PDMS (bottom). C) The transit and accumulated dose curve of the programmed delivery of fluoxetine is plotted. The wearable bioelectronic device delivers 30 µg of fluoxetine over 6 h and repeats daily. D) Schematics of the ion pumping process show that the electric field drives the fluoxetine cations (green spheres) to the wound through the ion-selective hydrogel (light yellow).

dose improves healing in a mouse wound model when topically applied to the wound bed.<sup>[13b,14]</sup> A blinking LED on the bioelectronic device indicated successful delivery (Figures S6 and S7, Movie S1, Supporting Information).

We used a previously reported machine-learning algorithm<sup>[17]</sup> to analyze images of wound size and area as an indication of wound healing progression (Figure 3D,E). Both the control and fluoxetine-treated wounds slightly increased in size at day 1 and decreased in size on subsequent days - this trend is expected in the process of wound healing (Figure 3F). There was no statistically significant difference in wound area between the treated wounds and the control. Therefore, we further assessed the wound healing process by measuring re-epithelialization on fully excised and fixed wounds, stained with hematoxylin and eosin (H&E) (Figure 3G,H; Figure S8, Supporting Information). Re-epithelialization, contributed to by both keratinocyte proliferation and migration, is required for wound closure.<sup>[18]</sup> Treatment of wounds with FLX<sup>+</sup> delivered from the bioelectronic device resulted in a 39.9% ( $P<0.05$ ) increase in re-epithelialization compared to control (Figure 3I), indicating a significant improvement in early-stage healing. To determine the actual drug delivery to the wound, we used an established method that utilizes the correlation between dose and charge in the ion pump.<sup>[19]</sup> By calculating the pump efficiency from in vitro results, we were able to derive the actual amount of fluoxetine delivered to each wound.<sup>[5b]</sup> Due to blood flow in the wound and drug half-life, measuring the drug concentration in the wound itself is challenging; how-

ever, leveraging the ion pump's characteristics allowed us to calculate and quantify the amount of drug delivered based on the measured current on each wound. Across 15 mice, the bioelectronic device consistently delivered the desired dose (Figure 3J, left). The variability in the delivered dose is primarily attributed to system-related factors, such as changes in contact resistance during mouse movement, rather than being intentional by design. Nonetheless, we leveraged this variability to establish a qualitative correlation between the dose of FLX<sup>+</sup> and wound healing, assessed by the percentage of re-epithelialization (Figure 3J, right). For example, re-epithelialization in mouse 2, which received >300 nMol per day FLX<sup>+</sup>, was much faster than in mouse 15, which received a 10x smaller dose. This observation is consistent with the direct topical application of fluoxetine to murine skin wounds.<sup>[13b,14]</sup> To enhance precision and minimize variability, we can implement a current control system with closed-loop control algorithms, as demonstrated in vitro with other ion pump systems.<sup>[20]</sup> These approaches can reduce variability and improved precision in drug delivery in future design of bioelectronic devices.

After analyzing the promising re-epithelialization data, we examined another crucial indicator of wound healing: the M1/M2 macrophage ratio (Figure 4).<sup>[21]</sup> Macrophages play a pivotal role in the immune response and are crucially involved in the healing and regeneration of wounds. Although macrophages are phenotypically heterogeneous over a continuum, a simplified classification based on their polarized functions during the

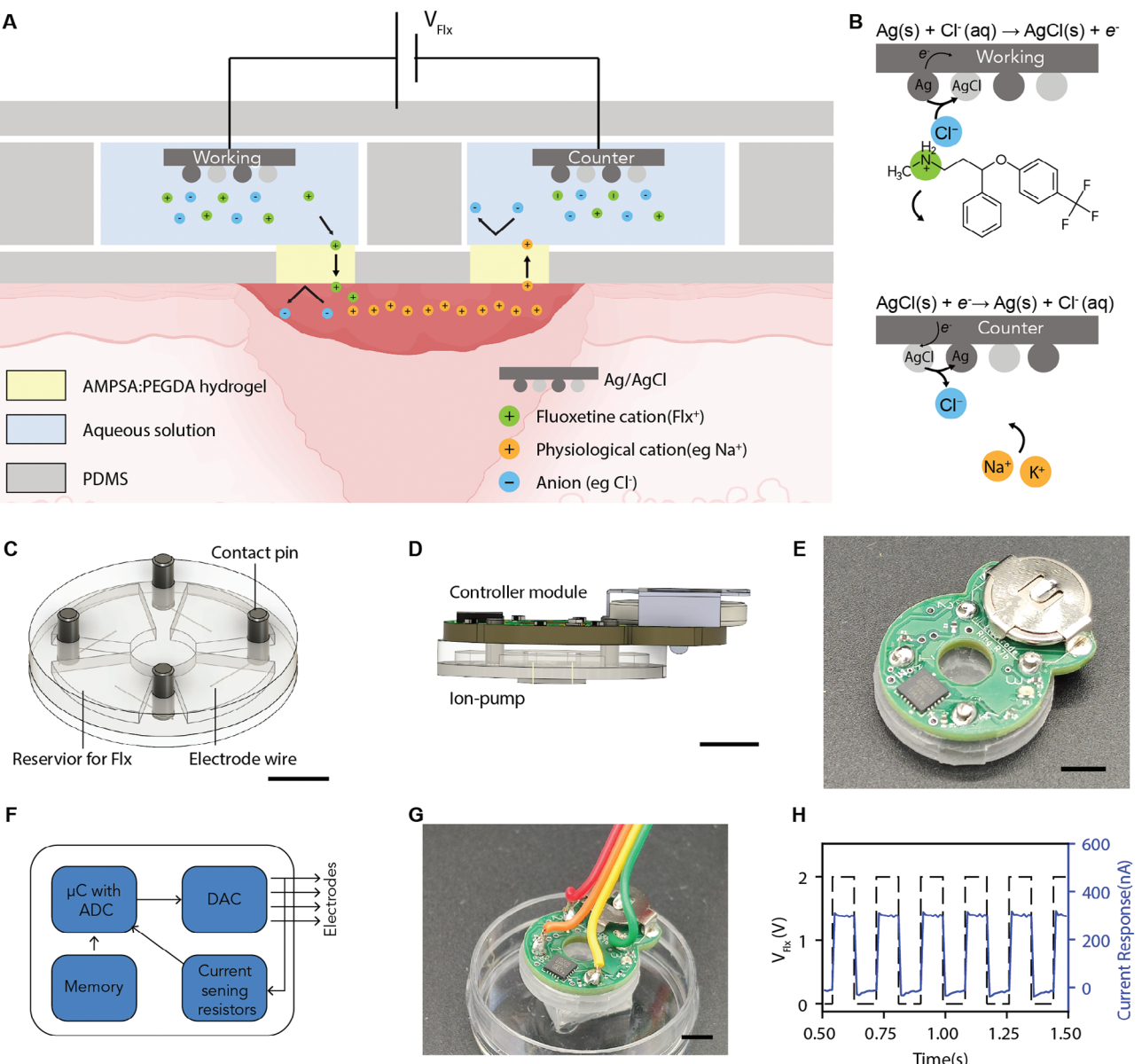


**Figure 2.** Showcases the design and characterization of the wearable bioelectronic devices. A) The ion pump's working principle is illustrated, where the reservoirs are filled with 0.01 M fluoxetine hydrochloride ( $\text{FLX}^+ \text{Cl}^-$ ) solution. Under positive  $V_{\text{Flx}}$ , the  $\text{FLX}^+$  cations migrate from the reservoir to the wound under electrophoretic force and exchange with physiological cations. An ion selective AMPSA:PEGDA polyanion hydrogel (light yellow) is negatively charged, acting as a filter that blocks anions such as  $\text{Cl}^-$ , while allowing cations such as  $\text{FLX}^+$  to pass. B) The electrochemical reaction for the ion pump electrodes is depicted happening at the opposite direction simultaneously. The Ag on the working electrode (gray) becomes oxidized under the electrochemical reaction, absorbs a  $\text{Cl}^-$  from the  $\text{FLX-HCl}$  solution, releases an electron, and becomes  $\text{AgCl}$ . This reaction releases an electron to the external circuit and leaves a free  $\text{FLX}^+$  cation. The  $\text{FLX}^+$  then migrates to the wound under electrophoretic force. The cathode reaction consumes an electron and releases a free  $\text{Cl}^-$ , which can balance with the incoming cation. C) A CAD model of the ion pump, made from PDMS. The ion pump has four reservoirs for fluoxetine solution, where electrode wires made from Ag and  $\text{AgCl}$  are inserted and connected to the external circuit through contact pins made of steel. Scale bar = 5 mm. D) CAD models of the wearable bioelectronic device device assembly, with the controller module on top and the ion pump on the bottom, are displayed. Scale bar = 5 mm. E) A camera photo of the wearable bioelectronic device is presented. Scale bar = 5 mm. F) The circuit diagram of the controller module is provided. It includes a microcontroller with a built-in clock and analog-to-digital converter (ADC), a memory chip, a digital-to-analog converter (DAC), and resistors for sensing current. G) A camera photo of the ex-vivo test setup for the wearable bioelectronic device while the device is in contact with the saline solution inside a PDMS well is shown. Scale bar = 5 mm. H) Plot of current response to a 2 V (peak to peak) square wave.

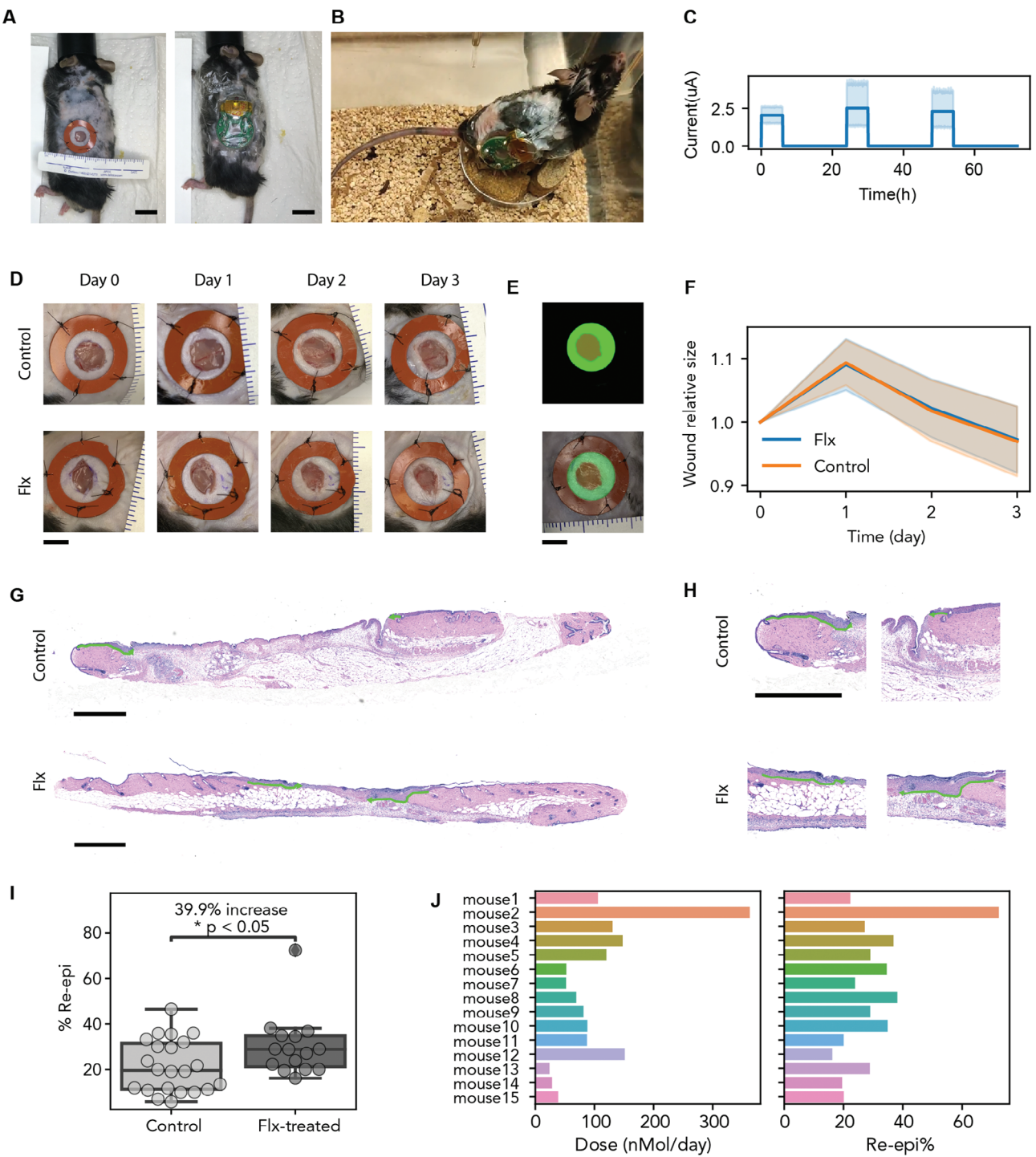


**Figure 3.** In vivo experiment of wearable bioelectronic device on mice. A) Photo of a mouse wound model during surgery. The left panel shows the mouse wound sutured with a silicone splint ring, and the right panel shows the wearable bioelectronic device fixed on the wound by Tegaderm. Scale bar = 5 mm. B) A mouse maintains normal daily activity while wearing the bioelectronic device on its wound. C) Plot of fluoxetine delivery over time from 15 experimental mice. D) Wound image taken from a group of experiments over 3 days. Scale bar = 5 mm. E) Image processing using machine learning to determine wound size. The top image is the mask generated by the algorithm to mark the size of the wound, and the bottom image depicts the overlayed image of the mask and the wound, showing that the masked area is accurate. F) Wound area analysis of the control group (orange line) and fluoxetine-treated group (blue line). G) H&E staining of tissue section across the wound. The top panel shows the control wound, and the bottom panel shows the fluoxetine-treated wound. The green line shows re-epithelialization. Scale bar = 1 mm. H) A zoomed-in view of the H&E staining on the area of the wound edge. Scale bar = 1 mm. I) Box plot of statistics of the re-epithelialization percentage of the wound. The control group ( $n = 22$ ) has  $22 \pm 12\%$  re-epithelialization, and the fluoxetine-treated group ( $n = 15-22$  mice,  $p < 0.05$ ) has  $30 \pm 14\%$  re-epi. J) Bar plot of dose versus re-epithelialization percentage on each fluoxetine-treated mouse.

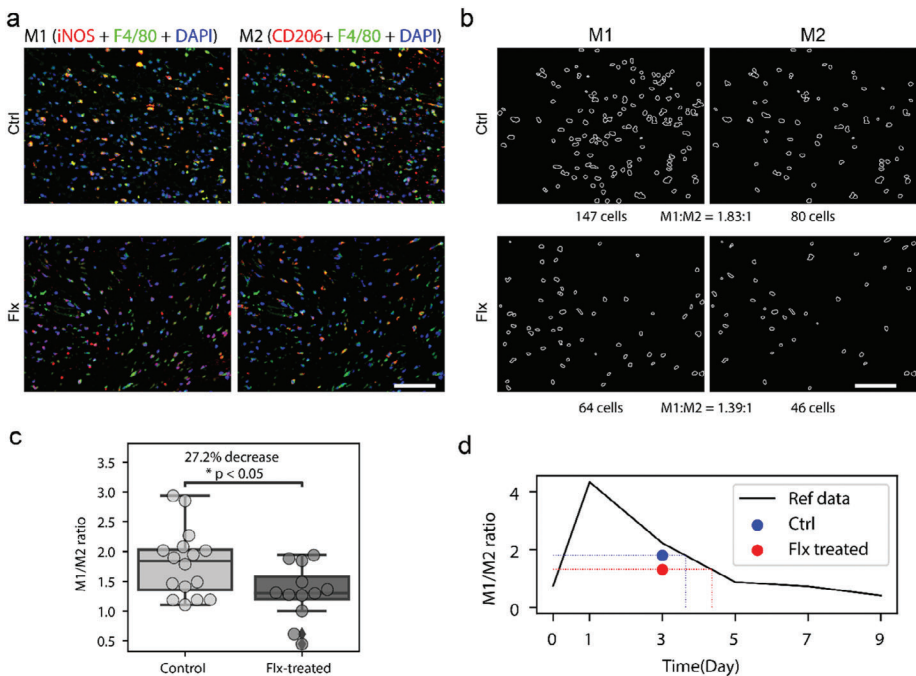


**Figure 4.** Macrophage analysis of the wound. A) Staining of different macrophage subtypes in the wound section. All cells (stained by DAPI, shown in blue), M1 (stained by iNOS, shown in red in left column), M2 (stained by CD206, shown in red in right column), and overall macrophages (stained by F4/80, shown in green) were imaged and presented. B) M1 and M2 cell count result from cross-channel counting, showing the distribution and ratio of macrophage subtypes, cell edges highlighted to separate individual cells. Scale bar = 200  $\mu\text{m}$ . C) Box plot showing statistics of the M1/M2 ratio, which was  $1.8 +/- 0.6$  in the control group and  $1.3 +/- 0.5$  for the fluoxetine-treated group. The fluoxetine-treated wounds ( $n = 13$  mice) demonstrated an average of 27.2% decrease in M1/M2 ratio compared to control wounds ( $n = 16$  mice),  $p < 0.05$ . D) Plot of the M1/M2 ratio over time. The blue dot represents the M1/M2 ratio from the control group, and the red dot represents the fluoxetine-treated group. The dashed lines indicate the projected wound age, while the solid line represents the trend plotted from the data in the reference.<sup>[25]</sup>

different stages of wound repair<sup>[21]</sup> defines the M1 subtype that carries out pro-inflammatory activities<sup>[22]</sup> and the M2 subtype that is anti-inflammatory<sup>[23]</sup> and promotes tissue repair.<sup>[24]</sup> Using immunohistochemistry to identify the subtypes based on the expression of recognized markers, we found M1 macrophages significantly infiltrated the center of the control wound three days after injury, while there was no change observed in the fluoxetine-treated wound (Figure 4A; Figure S9, Supporting Information). Meanwhile, the number of M2-like macrophages increased in the center of the fluoxetine-treated wound, as depicted in Figure 4A. At day 3 the M1/M2 ratio was noticeably reduced following treatment, as shown in the overlay of M1 and M2 cells (Figure 4B). Fluoxetine treatment additionally reduced the M1/M2 ratio on day 3 by 27.2% compared to the control ( $P < 0.05$ ) (Figure 4C) indicating a lower number of the M1 pro-inflammatory macrophages compared to the M2 pro-reparative macrophages. This M1/M2 ratio decrease suggests a shorter inflammatory phase with a more rapid progression toward the reparative phase of healing, consistent with the noted improvement in wound re-epithelialization.

To further investigate this effect, we examined the M1/M2 ratio change in the context of a continuous curve over the healing process. Using time series data of M1 and M2 cells in mouse incision wounds obtained from published studies,<sup>[25]</sup> we plotted the M1/M2 ratio's dependence on time (Figure 4D). Though the comparison of the published data generated from incisional wounds<sup>[25]</sup> to the current data generated from excisional wounds may be an imperfect approach, nevertheless, plotting M1/M2 ra-

tio along with published data enables us to estimate the wound progression. The M1/M2 ratio of both fluoxetine-treated and control wounds on day 3 of this experiment are within the same order of magnitude (blue and red dots in Figure 4D) as the time-series obtained from published data (black line in Figure 4D). However, because the curve is non-monotonic, there are two periods that might correspond to the M1/M2 value obtained in this study – one is day 0, and another is days 3–5. After taking into account other wound indicators, such as the onset of re-epithelialization, the presence of macrophages, and diminishing wound size, we conclude that our day 3 data correspond to the day 3–5 part of the curve, i.e., M1/M2 ratio is monotonically decreasing in that time period. Therefore, a lower M1/M2 ratio indicates that the wound has entered a later healing stage. Previous studies reported that the M1-M2 transition is critical for the resolution of inflammation and for promoting tissue repair.<sup>[26]</sup> Since the fluoxetine-treated wounds showed increased re-epithelialization and decreased M1/M2 ratio, we conclude that we have demonstrated proof of concept that the wearable bioelectronic device's fluoxetine treatment accelerated the wound-healing process. This finding is consistent with earlier studies that directly applied fluoxetine to the wound bed.<sup>[13b,14]</sup> Although fluoxetine is a selective serotonin reuptake inhibitor primarily used as a systemically administered drug for treating depression, recent studies that identify serotonin receptors in the epidermal cells reveals the potential of SSRI drugs to facilitate wound healing.<sup>[27]</sup> Topical application of fluoxetine, either in solution

or in a hydrogel, improves wound healing in diabetic and non-diabetic rodent skin,<sup>[13c,28]</sup> and minimizes infection,<sup>[29]</sup> possibly via regulating the local serotonin pathway to promote keratinocyte migration and modulate inflammatory responses.<sup>[13b]</sup> Similarly, fluoxetine has been reported to increase M2, anti-inflammatory phenotype in microglial macrophages in vitro.<sup>[30]</sup> These effects collectively can contribute to improved skin wound healing.

We have engineered a wearable bioelectronic device for continuous delivery of treatment to the wound. This treatment limits the need for patient self-delivered daily topical treatment that may be error-prone in terms of dose and complicated by patient non-adherence.<sup>[31]</sup> Delivery from the bioelectronic device also minimizes the potential for non-specific off-target effects since there is little to no systemic accumulation of fluoxetine or impact on the serotonin metabolism (Figure S10, Supporting Information)<sup>[32]</sup>. Finally, our analysis of a 7-day positive control with topical application of fluoxetine to the wound caused a decrease of re-epithelialization on mice (Figure S11, Supporting Information). Bioelectronic treatment with fluoxetine, on the other hand, resulted in a 39.9% increase of re-epithelialization at day 3 brings a huge benefit. Furthermore, with this precise delivery system, it may be possible to deliver drugs with temporal targeting of specific sub-populations of immune cells or epithelial cells as they emerge at the wound site for tissue repair.

As this research is a proof of concept for the in vivo application of wearable bioelectronic devices for drug delivery, the sample size is small, and the treatment duration is short, resulting in a wide distribution in experimental outcomes. Also, we only used the bioelectronic device to deliver a pre-determined dosage repetitively instead of delivering a customized treatment regimen. Though we proved that bioelectronic drug delivery helped wound healing compared to no treatment, additional studies to compare it with other drug delivery methods, such as bolus topical application or conventional gradual release encapsulations, are needed to fully demonstrate the advantage of the wearable bioelectronic devices.

We selected fluoxetine as the test drug for delivery, but the strategy of wearable bioelectronic ion pump devices can also be used for other charged biomolecules, such as acetylcholine.<sup>[33]</sup> Moreover, neutral molecules like gamma-aminobutyric acid (GABA) can be converted into charged ions under certain pH conditions and delivered through bioelectronic ion pumps.<sup>[4a,5a,16]</sup> We primarily employed histological staining techniques, specifically re-epithelialization evaluation through H&E staining,<sup>[18d,34]</sup> and macrophage phenotype assessment through immunohistochemical marker staining,<sup>[10a,35]</sup> to monitor the wound healing process. These methods are widely recognized, well-established, and commonly utilized in research. It is worth noting that more advanced techniques, such as Imaging Mass Cytometry (IMC) offer the potential to provide greater detail and improved accuracy for future investigations.<sup>[36]</sup> As a proof-of-concept study, we utilized a total of 34 mice, all of which were sacrificed on day 3 to facilitate statistical analysis. However, considering that day 3 data represents only a single time point, a study with a larger sample size distributed over various time points would yield more conclusive results.

### 3. Conclusion

Our results demonstrate the successful design and fabrication of a wearable bioelectronic device capable of actively controlling drug release for in vivo wound healing. The device is standalone, and it includes an ion pump delivery module, a controller module, and a power supply, eliminating the need for external instruments or connections to operate. This configuration allows for extended periods of use without external interaction. We created a wound treatment that provides the timed and programmed delivery of fluoxetine in a mouse wound model, and if used clinically, would not require patient intervention. Our treatment resulted in faster wound healing at day 3 as indicated by a statistically significant 39.9% increase in re-epithelialization and 27.2% decrease in M1 pro-inflammatory macrophages respect to M2 pro-reparative macrophages. These results suggest that delivery of fluoxetine from the wearable bioelectronic device promotes wound healing by influencing the balance of M1/M2 phenotypes and keratinocyte migration. While the effect of fluoxetine accelerating wound healing is not surprising, the wearable bioelectronic device offers a customized drug dose regimen with temporal precision, which can be favorable over the conventional systemic routes of drug administration that deliver a single, full dose every 24 h with an initial peak and subsequent lower concentration. In future research, the timing of drug release can be programmed to align with the wound stage<sup>[37]</sup> in a closed loop fashion<sup>[38]</sup> to further aid the healing process. We aim to further optimize the design of the wearable bioelectronic device for potential clinical use in the future.

### 4. Experimental Section

**Experimental Design:** The objective of this experimental research is to evaluate the effectiveness of a wearable bioelectronic device with an integrated electrophoretic ion pump for programmable drug delivery and enhanced wound healing in mice. It is hypothesized that the device could deliver drugs with precise dose control and personalized therapeutic profiles to wounds in mice, leading to faster overall healing with minimal side effects.

The wearable bioelectronic device was tested in vivo using a mouse wound model. A total of 37 male C57BL/6J mice were used, with 15 in the treatment group and 22 in the control group. Six-millimeter wounds were created on the back of each mouse under anesthesia, using the protocol we have previously reported.<sup>[13b]</sup> The control group received a wearable bioelectronic device that was not powered on, while the treatment group received 6 h of fluoxetine delivery per day for 3 days. The wound area, re-epithelialization rate, and M1/M2 macrophage ratio were evaluated using digital photography and histological analysis.

**Design of Wearable Bioelectronic Device:** The wearable bioelectronic device comprises two major components: the delivery module or ion pump, and the controller module with a PCB, electronic components, and a battery. These components were fabricated separately and then assembled.

**Fabrication of Ion Pump:** To fabricate the ion pump for the wearable bioelectronic device, AutoCAD software was used to design 3D-printed, two-part molds (Figure S1a, Supporting Information). The molds were filled with Polydimethylsiloxane (PDMS) and baked at 60 °C for 48 h. The resulting PDMS parts were then removed from the molds (Figure S1b, Supporting Information) and cleaned with Isopropyl Alcohol (IPA) and water, followed by nitrogen ( $N_2$ ) drying to ensure no debris remained on the PDMS layers. The top layer of PDMS contained four reservoirs,

designed to hold fluoxetine solutions of specific concentrations, and four capillary tubes filled with hydrogels for fluoxetine delivery. The bottom PDMS part acted as a lid, covering the reservoirs and featuring a 0.5 mm tall notch to ensure contact with the wound bed below the skin. Ag and Ag/AgCl wires with a diameter of 0.1 mm were inserted inside each reservoir. The top and bottom layers were bonded together through oxygen ( $O_2$ ) plasma treatment, which oxidizes the polymer surface and changes the  $CH_3$  groups on the PDMS surface to OH groups. The oxidized surfaces were bonded together using custom aluminum pieces. The PDMS surface was coated with Parylene to increase the media lifetime on the PDMS reservoirs. Hydrogel-filled capillaries, which act as the ion exchange membrane for the ion pump, were fabricated using a previously optimized and reported method.<sup>[39]</sup> The hydrogel recipe in this study consisted of a 1 M concentration of 2-acrylamido-2-methyl-1-propanesulfonic acid (AMPSA), 0.4 M concentration of polyethylene glycol diacrylate (AMPSA), and 0.05 M concentration of photoinitiator (I2959). 100 mm of silica tubing with an inner diameter of 100  $\mu m$  and an outer diameter of 375  $\mu m$  were etched with NaOH and then treated with silane A174 to prevent hydrogel expansion. The hydrogel was cross-linked with five minutes of 365 nm UV treatment at a power density of 8 mW  $cm^{-2}$ . After UV curing, the capillary tubes were segmented into 5 mm segments and loaded by immersing them in a 0.01 M fluoxetine solution for at least 4 h before use. Finally, the capillaries filled with hydrogel were inserted into each reservoir to complete the fabrication of the ion pump.

**Design and Fabrication of Controller Module:** The controller module for drug delivery comprises a programmable PCB with electronic components used for actuation and sensing. The PCB was designed using Autodesk EAGLE and contains a microcontroller with a built-in ADC, a memory chip, a DAC, and resistors for sensing current (Figure 2F). Prior to the experiment, programs were flashed into the onboard microcontroller, and actuation commences automatically once the battery is inserted. During program execution, the microcontroller sent I<sub>C</sub> commands to the DAC to apply the appropriate voltages to the electrodes of the ion pump. As a result, current flowed through the resistors, generating voltages that could be read by either the ADC on the microcontroller or by external probes.

**Assembling of the Wearable Bioelectronic Device:** To integrate the two modules of the wearable bioelectronic device, steel pins were inserted into four holes on the PDMS layer of the ion pump. The bottom of each pin was coated with silver paste to establish electrical connections between the pin and Ag or Ag/AgCl electrodes. After assembling the wearable bioelectronic device, the pins were soldered to the PCB. Sterilized fluoxetine hydrochloride solutions (0.01 M) were then prepared by dissolving the drug in sterilized water, adjusting the pH to 6 to allow the fluoxetine to protonate, filtering through 0.2  $\mu m$  filters, and injecting the sterilized fluoxetine solutions into each reservoir.

**Ex vivo Testing of the Wearable Bioelectronic Device:** The wearable bioelectronic device was tested ex vivo in PDMS wells filled with Steinberg solution to mimic the biochemical environment of tissue. The testing involved connecting the wearable bioelectronic device to a potentiostat (Metrohm Autolab) and controlling the voltage pattern via a computer while the ion pump outlet contacted the solution in the well. After a specific duration of actuation, voltage and current were recorded, and the test was stopped to collect the solution in the well. The total charge that went through the circuit was calculated by integrating the current over time, and the dose of fluoxetine was calculated by HPLC-MS. The efficiency of the delivery  $\eta = \text{moles of fluoxetine}/\text{moles of charge}$ .

**Measurement of Fluoxetine with HPLC-MS:** In order to measure the concentration of fluoxetine in the solution, we utilized HPLC-MS (Thermo Scientific LTQ) with a reversed-phase column (Syngi 4  $\mu m$  Fusion-RP 80  $\text{\AA}$ , 150  $\times$  2 mm, 00F-4424-B0). Initially, we generated a standard curve from a series of samples with known concentrations of fluoxetine. These samples were then analyzed using HPLC-MS to verify the fluoxetine peak by retention time and mass reading, and the mass-spec intensity was recorded. The peak area of mass-spec intensity versus concentration was plotted in (Figure S4, Supporting Information) and fitted the data to a calibration curve to obtain the slope and intercept. Subsequently, the collected samples with unknown concentrations were loaded into the

HPLC-MS and we recorded the fluoxetine intensity. Using the peak area and calibration curve, we were able to calculate the concentration of the sample.

**Mouse Preparation and Drug Delivery by the Wearable Bioelectronics Device:** The device was tested on C57BL/6J male mice by creating full-thickness, 6 mm circular wounds on their backs.<sup>[13b]</sup> Bioelectronics devices were then applied with either fluoxetine (experimental group, 15 mice) or a mock control device (on control group, 22 mice) to the wounds and secured them with a Tegaderm overwrap. The target delivery dose for fluoxetine was set at 100 nMol or 0.035 mg  $wound^{-1} day^{-1}$  during the daily 6 h delivery program. On the third day after the surgery, we removed the wearable bioelectronic devices, captured images of the wounds using a camera, and harvested wound tissue for histological analysis.

**Tissue Collection and Sectioning:** After euthanizing the mice at the end of each experiment, wounds were excised and placed in a paraformaldehyde solution for fixation for 24 h. Fixed tissues were then processed in a tissue processor for formalin-fixed paraffin-embedded (FFPE) tissue histology. During processing, the tissues were dehydrated and impregnated with paraffin wax to preserve the tissue structure. The processed tissues were embedded into paraffin blocks and cut into 5  $\mu m$  thick sections using a microtome, and the sections were placed onto glass slides. After drying, these sections were used for further analysis of re-epithelialization and macrophage subtypes.

**Re-Epithelialization Calculation:** To assess re-epithelialization, tissue sections were stained with H&E using a standard protocol. Brightfield images were taken on a BioRevo BZ-9000 inverted microscope, and BZ Analyzer software (Keyence, Osaka, Japan) was used to score the images. The left and right wound edges were determined by identifying the innermost follicle on each side. The basal keratinocyte layer was used to measure epithelial ingrowth on each side of the wound, from the innermost follicle to the tip of the epithelial tongue. The total width of the wound was measured along the surface of the granulation tissue between the two follicles. The percent re-epithelialization was calculated as [(length of left epithelial tongue in  $\mu m$ ) + (length of right epithelial tongue in  $\mu m$ )]/(wound width in  $\mu m$ )  $\times$  100.

**Macrophage Staining:** Full-thickness mouse skin tissues were collected from both fluoxetine-treated and untreated groups 3 days after wounding and examined them for the expression of M1 (F4/80+iNOS+) and M2 (F4/80+CD206+) macrophage markers. To detect all macrophages, F4/80 as a pan-macrophage marker was used. M1-like macrophages were identified as a fraction of F4/80+ macrophages expressing inducible nitric oxide synthase (iNOS), and M2-like macrophages as F4/80+ cells expressing CD206.

Formalin-fixed, paraffin-embedded tissues were deparaffinized, processed for antigen retrieval, and blocked for 2 h at room temperature with 10% Donkey Serum (Thermo Fisher). The slides were then incubated overnight at 4 °C with primary antibodies, including Rat anti-F4/80 (dilution 1:50; MCA497G, BIO-RAD, Hercules, CA), Rabbit anti-iNOS (dilution 1:100; PA3-030A, Thermo Fisher Scientific), and Goat anti-CD206 (dilution 1:100; PA5-46994, Thermo Fisher Scientific). These antibodies were selected based on the validation information provided on the manufacturers' websites. Some samples with technical problems with staining were excluded, leaving 13 samples for FLX-treated group and 16 for control group for scoring.

After washing, sections were incubated with corresponding Alexa Fluor-conjugated secondary antibodies (Donkey Anti rat-AlexaFluor 488, Donkey Anti rabbit-AlexaFluor 647, Donkey Anti goat-AlexaFluor 568, dilution 1:200, Thermo Fisher Scientific). Nuclei were counterstained with 4',6-diamidino-2-phenylindole (DAPI), and coverslips were mounted using an anti-fade mountant (SlowFade Mountant; S36936, Thermo Fisher Scientific). Fluorescence images were acquired using a Keyence automated high-resolution microscope (BZ-X800, KEYENCE, Itasca, IL). Five adjacent areas were imaged at the wound center at 40x magnification and processed the images using ImageJ and CellProfiler 4.2 software.

For semi-quantification, the numbers of macrophage subtypes in the wound were manually counted based on double-positive staining with

F4/80+iNOS+ for M1-like macrophages and F4/80+CD206+ for M2-like cells, with blind evaluation.

**Fluoxetine Quantitative Analysis in Blood:** To measure the levels of fluoxetine and its major metabolite norfluoxetine in mouse serum, reverse-phase HPLC was employed with UV detection and purified the samples using C18 pipette-tip solid phase extraction (C18 PT-SPE). The mobile phase used was 300:700:1 acetonitrile: 50 mM phosphate buffer pH 6.0: triethylamine. Separation of fluoxetine, norfluoxetine, and fluvoxamine (the internal standard) was achieved on a Cortecs C18 column (3 mm ID × 100 mm L, 2.7 μm particle diameter, Waters, Ireland) at a flow rate of 450 μL min<sup>-1</sup> and a temperature of 35 °C. The column effluent was monitored at 230 nm with a time constant of 0.5 s. For the PT-SPE cartridges, 20 mg C18 silica sorbent was slurry-packed in methanol into 1 mL pipette tips using glass wool as a bottom frit, and acid-washed sand in place of a top frit. After packing, 2 tube volumes of water were passed through and the cartridges were ready for use. To prepare the sample loading solution, 10 μL of a fluvoxamine solution (10 μg mL<sup>-1</sup> in methanol) was spiked into 100 μL of study serum, and then diluted this solution with 100 μL of water. This sample loading solution was applied to the conditioned SPE cartridges, which were then washed with 600 μL ultra-pure water followed by 600 μL 50:50 methanol:water. Fluoxetine, norfluoxetine, and fluvoxamine were eluted using 100 μL of methanol containing 0.5% (v/v) formic acid. After elution, we diluted the samples 1:1 with water, mixed well, and centrifuged them. Finally, 10 μL of the resulting solution was injected for analysis.

**Serotonin Quantitation in Blood:** Serotonin quantitation in mouse serum was performed according to the previously published protocol.<sup>[40]</sup>

**Statistical Analysis:** Statistical analysis was performed using multiple software packages including Microsoft Excel, the Scipy.stats library written in Python, and Prism 9. The significance of the comparison of re-epithelialization and M1/M2 ratio between the treated and control group was assessed using an independent two-tailed Student's t-test, with a significance level of  $P < 0.05$ . The correlation between the dose and re-epithelialization is evaluated by Pearson correlation coefficient ( $r$ ), where  $r^2 > 0.5$  is considered a strong correlation. The significance of the linear regression was evaluated by Wald Test with t-distribution, with a significance level of  $P < 0.05$ .

**Ethical Statement for Animal Experiment:** All animal experiments conducted in this study were approved by the Institutional Animal Care and Use Committee (IACUC) at the University of California, Davis, under an approved protocol. The animal handling protocol was designed to minimize pain or discomfort to the animals, and the study adheres to UC Davis and Federal ethical and regulatory guidelines.

## Supporting Information

Supporting Information is available from the Wiley Online Library or from the author.

## Acknowledgements

The authors thank the help from Mr. Vincent Pham and Dr. Harrison Shawa for assisting the mouse experiments and animal care. The authors thank the help from Dr. Chuong Nguyen for assisting the mouse experiments and analyzing the data. The authors thank the help from DaVinci Biomedical Research Products, Inc. For conducting the biocompatibility test of the device on rabbits. This research was sponsored by the Defense Advanced Research Projects Agency (DARPA) through Cooperative Agreement D20AC0003 awarded by the U.S. Department of the Interior (DOI), Interior Business Center. The content of the information does not necessarily reflect the position or the policy of the Government, and no official endorsement should be inferred.

## Conflict of Interest

The authors declare no conflict of interest.

## Author Contributions

H.L. and H.Y. contributed equally to this work. H.L., H.Y., M.T., R.I., M.R., and J.S. performed conceptualization. H.L., H.Y., P.B., H.H., T.N., C.H., K.Z., J.S., L.L., H.C., M.T., M.A., L.L., A.B., J.O., C.H., and M.R. performed methodology. H.L., H.Y., N.A., P.B., A.L., A.G., K.Z., and C.R. performed investigation. H.L., K.Z., and H.C. performed visualization. R.I., M.R., M.T., M.Z., M.G., M.L., A.S., and N.N. performed supervision. H.L. and H.Y. wrote the original draft. H.L., H.Y., N.A., T.N., K.Z., M.T., M.Z., M.G., R.I., and M.R. wrote, reviewed, and edited the final manuscript.

## Data Availability Statement

The data that support the findings of this study are available in the supplementary material of this article.

## Keywords

bioelectronic ion pump, controlled drug delivery, wearables, wound healing

Received: July 28, 2023

Revised: November 6, 2023

Published online: February 5, 2024

- [1] L. S. Goodman, A. Gilman, L. L. Brunton, *Goodman & Gilman's manual of pharmacology and therapeutics*, McGraw-Hill Medical, New York 2008.
- [2] a) J. V. Natarajan, C. Nugraha, X. W Ng, S. Venkatraman, *J. Control Release* **2014**, 193, 122; b) T. Thambi, Y. Li, D. S. Lee, *J. Control Release* **2017**, 267, 57; c) Z. Hemmatian, E. Jalilian, S. Lee, X. Strakosas, A. Khademhosseini, A. Almutairi, S. R. Shin, M. Rolandi, *ACS Appl. Mater. Interfaces* **2018**, 10, 21782.
- [3] a) H. Joo, Y. Lee, J. Kim, J.-S. Yoo, S. Yoo, S. Kim, A. K. Arya, S. Kim, S. H. Choi, N. Lu, H. S. Lee, S. Kim, S.-T. Lee, D.-H. Kim, *Sci. Adv.* **2021**, 7, eabd4639; b) B. Mc Adams, A. Rizvi, *J. Clin. Med.* **2016**, 5, 5; c) R. Farra, N. F. Sheppard, L. McCabe, R. M. Neer, J. M. Anderson, J. T. Santini, M. J. Cima, R. Langer, *Sci. Transl. Med.* **2012**, 4, 122ra21; d) N. Di Trani, A. Silvestri, G. Bruno, T. Geninatti, C. Y. X. Chua, A. Gilbert, G. Rizzo, C. S. Filgueira, D. Demarchi, A. Grattoni, *Lab Chip* **2019**, 19, 2192.
- [4] a) X. Strakosas, M. Seitanidou, K. Tybrandt, M. Berggren, D. T. Simon, *Sci. Adv.* **2021**, 7, eabd8738; b) D. T. Simon, E. W. H. Jager, K. Tybrandt, K. C. Larsson, S. Kurup, A. Richter-Dahlfors, B. Berggren, in *TRANSDUCERS 2009 – 2009 International Solid-State Sensors, Actuators and Microsystems Conf.*, IEEE, Piscataway, NJ **2009**, pp. 1790–1793; c) M. P. Jia, H. Dechiruji, J. Selberg, P. Pansodtee, J. Mathews, C. X. Wu, M. Levin, M. Teodorescu, M. Rolandi, *Apl. Mater.* **2020**, 8, 091106; d) M. P. Jia, M. Jafari, P. Pansodtee, M. Teodorescu, M. Gomez, M. Rolandi, *APL Mater.* **2022**, 10, 041112.
- [5] a) C. M. Proctor, A. Slézia, A. Kaszas, A. Ghestem, I. Del Agua, A.-M. Pappa, C. Bernard, A. Williamson, G. G. Malliaras, *Sci. Adv.* **2018**, 4, eaau1291; b) I. Uguz, C. M. Proctor, V. F. Curto, A.-M. Pappa, M. J. Donahue, M. Ferro, R. M. Owens, D. Khodagholy, S. Inal, G. G. Malliaras, *Adv. Mater.* **2017**, 29, 1701217; c) A. Jonsson, T. A. Sjöström, K. Tybrandt, M. Berggren, D. T. Simon, *Sci. Adv.* **2016**, 2, e1601340.
- [6] M. Zhao, M. Rolandi, R. R. Isseroff, *Cold Spring Harb Perspect Biol.* **2022**, 14, a041236.
- [7] a) R. W. Tarnuzzer, G. S. Schultz, *Wound Repair Regen* **1996**, 4, 321; b) D. R. Yager, R. A. Kulina, L. A. Gilman, *The Int. J. Lower Extremity Wounds* **2007**, 6, 262.

- [8] a) D. Y. Matar, B. Ng, O. Darwish, M. Wu, D. P. Orgill, A. C. Panayi, *Adv. Wound Care* **2023**, *12*, 269; b) P. Martin, *Science* **1997**, *276*, 75; c) S. Willenborg, L. Injarabian, S. A. Eming, *Cold Spring Harb Perspect Biol* **2022**, *14*, a041216.
- [9] V. Falanga, R. R. Isseroff, A. M. Soulka, M. Romanelli, D. Margolis, S. Kapp, M. Granick, K. Harding, *Nat. Rev. Dis. Primers* **2022**, *8*, 50.
- [10] a) Y. Jiang, A. A. Trotsuk, S. Niu, D. Henn, K. Chen, C.-C. Shih, M. R. Larson, A. M. Mermin-Bunnell, S. Mittal, J.-C. Lai, A. Saberi, E. Beard, S. Jing, D. Zhong, S. R. Steele, K. Sun, T. Jain, E. Zhao, C. R. Neimeth, W. G. Viana, J. Tang, D. Sivaraj, J. Padmanabhan, M. Rodrigues, D. P. Perrault, A. Chattopadhyay, Z. N. Maan, M. C. Leeolou, C. A. Bonham, S. H. Kwon, et al., *Nat. Biotechnol.* **2022**, *1*, 652; b) C. Wang, X. Jiang, H.-J. Kim, S. Zhang, X. Zhou, Y. Chen, H. Ling, Y. Xue, Z. Chen, M. Qu, L. Ren, J. Zhu, A. Libanori, Y. Zhu, H. Kang, S. Ahadian, M. R. Dokmeci, P. Servati, X. He, Z. Gu, W. Sun, A. Khademhosseini, *Biomaterials* **2022**, *285*, 121479.
- [11] P. Mostafalu, G. Kiaee, G. Giatsidis, A. Khalilpour, M. Nabavina, M. R. Dokmeci, S. Sonkusale, D. P. Orgill, A. Tamayol, A. Khademhosseini, *Adv. Funct. Mater.* **2017**, *27*, 1702399.
- [12] M. L. García-García, C. A. Tovilla-Zárate, M. Villar-Soto, I. E. Juárez-Rojop, T. B. González-Castro, A. D. Genis-Mendoza, M. Á. Ramos-Méndez, M. L. López-Návarez, A. S. Saucedo-Osti, J. A. Ruiz-Quiñones, J. J. Martínez-Magaña, *Psychiatry Res.* **2022**, *307*, 114317.
- [13] a) R. M. Z. Farahani, K. Sadr, J. S. Rad, M. Mesgari, *Adv. Skin Wound Care* **2007**, *20*, 157; b) C. M. Nguyen, D. M. Tartar, M. D. Bagood, M. So, A. V. Nguyen, A. Gallegos, D. Fregoso, J. Serrano, D. Nguyen, D. Degovics, A. Adams, B. Harouni, J. J. Fuentes, M. G. Gareau, R. W. Crawford, A. M. Soulka, R. R. Isseroff, *Diabetes* **2019**, *68*, 1499; c) N. A. Alhakamy, G. Caruso, A. Privitera, O. A. A. Ahmed, U. A. Fahmy, S. Md, G. A. Mohamed, S. R. M. Ibrahim, B. G. Eid, A. B. Abdel-Naim, F. Caraci, *Pharmaceutics* **2022**, *14*, 1133.
- [14] D. J. Yoon, C. Nguyen, M. D. Bagood, D. R. Fregoso, H.-Y. Yang, A. I. Medina Lopez, R. W. Crawford, J. Tran, R. R. Isseroff, *J. Invest. Dermatol.* **2021**, *141*, 1608.
- [15] N. J. Trengove, S. R. Langton, M. C. Stacey, *Wound Repair Regen.* **1996**, *4*, 234.
- [16] M. Seitanidou, J. F. Franco-Gonzalez, T. A. Sjöström, I. Zozoulenko, M. Berggren, D. T. Simon, *J. Phys. Chem. B* **2017**, *121*, 7284.
- [17] H. Carrión, M. Jafari, M. D. Bagood, H.-Y. Yang, R. R. Isseroff, M. Gomez, *PLoS Comput. Biol.* **2022**, *18*, e1009852.
- [18] a) H.-Y. Yang, F. Fierro, D. J. Yoon, A. Gallegos, S. L. Osborn, A. V. Nguyen, T. R. Peavy, W. Ferrier, L. Talken, B. W. Ma, K. G. Galang, A. Medina Lopez, D. R. Fregoso, H. Stewart, E. A. Kurzrock, A. M. Soulka, J. A. Nolta, R. R. Isseroff, *J. Biomed. Mater. Res. B Appl. Biomater.* **2022**, *110*, 1615; b) H.-Y. Yang, F. Fierro, M. So, D. J. Yoon, A. V. Nguyen, A. Gallegos, M. D. Bagood, T. Rojo-Castro, A. Alex, H. Stewart, M. Chigbrown, M. R. Dasu, T. R. Peavy, A. M. Soulka, J. A. Nolta, R. R. Isseroff, *Stem Cells Transl. Med.* **2020**, *1353*, 1353 c) K. Ueno, S. Saika, Y. Okada, H. Iwanishi, K. Suzuki, G. Yamada, S. Asamura, *Exp. Anim.* **2022**, *72*, 224; d) R. D. Galiano, J. Michaels, M. Dobryansky, J. P. Levine, G. C. Gurtner, *Wound Repair Regener.* **2004**, *12*, 485; e) S. Erratico, M. Belicchi, M. Meregalli, D. Di Silvestre, L. Tripodi, A. De Palma, R. Jones, E. Ferrari, L. Porretti, E. Trombetta, G. R. Merlo, P. Mauri, Y. Torrente, *Cell. Mol. Life Sci.* **2022**, *79*, 259.
- [19] L. Waldherr, M. Seitanidou, M. Jakesová, V. Handl, S. Honeder, M. Nowakowska, T. Tomin, M. Karami Rad, T. Schmidt, J. Distl, R. Birner-Gruenberger, G. Von Campe, U. Schäfer, M. Berggren, B. Rinner, M. Asslaber, N. Ghaffari-Tabrizi-Wizsy, S. Patz, D. T. Simon, R. Schindl, *Adv. Mater. Technol.* **2021**, *6*, 2001302.
- [20] a) J. Selberg, M. Jafari, C. Bradley, M. Gomez, M. Rolandi, *APL Mater.* **2020**, *8*, 120904 b) H. Dechiraju, J. Selberg, M. P. Jia, P. Pansodtee, H. P. Li, H. C. Hsieh, C. Hernandez, N. Asefifeyzabadi, T. Nguyen, P. Baniya, G. Marquez, C. Rasmussen-Ivey, C. Bradley, M. Teodorescu, M. Gomez, M. Levin, M. Rolandi, *AIP Adv.* **2022**, *12*, 125205 c) J. Selberg, M. Jafari, J. Mathews, M. P. Jia, P. Pansodtee, H. Dechiraju, C. X. Wu, S. Cordero, A. Flora, N. Yonas, S. Jannetty, M. Diberardinis, M. Teodorescu, M. Levin, M. Gomez, M. Rolandi, *Adv. Intell. Syst.-Ger.* **2020**, *2*, 2000140.
- [21] a) D. M. Mosser, J. P. Edwards, *Nat. Rev. Immunol.* **2008**, *8*, 958; b) T. Lucas, A. Waisman, R. Ranjan, J. Roes, T. Krieg, W. Müller, A. Roers, S. A. Eming, *J. Immunol.* **2010**, *184*, 3964.
- [22] D. C. Dale, L. Boxer, W. C. Liles, *Blood* **2008**, *112*, 935.
- [23] a) M. M. Hunter, A. Wang, K. S. Parhar, M. J. G. Johnston, N. Van Rooijen, P. L. Beck, D. M. McKay, *Gastroenterology* **2010**, *1395*, 1395; b) S. K. Brancato, J. E. Albina, *Am. J. Pathol.* **2011**, *178*, 19.
- [24] S. Gordon, *Nat. Rev. Immunol.* **2003**, *3*, 23.
- [25] Y. Du, P. Ren, Q. Wang, S.-K. Jiang, M. Zhang, J.-Y. Li, L.-L. Wang, D.-W. Guan, *J. Inflamm.* **2018**, *15*, 25.
- [26] N. X. Landén, D. Li, M. Stähle, *Cell. Mol. Life Sci.* **2016**, *73*, 3861.
- [27] a) J. Wetterberg, C. Taher, E. C. Azmitia, H. El-Nour, *J. Eur. Acad. Dermatol. Venereol.: JEADV* **2011**, *25*, 1200; b) H.-H. Tang, Y.-F. Zhang, L.-L. Yang, C. Hong, K.-X. Chen, Y.-M. Li, H.-L. Wu, *FASEB J.: Offic. Publcat. Feder. American Socie. Experi. Biol.* **2023**, *37*, e22893; c) K. Nordlund, K. Thorslund, S. Lonne-Rahm, S. Mohabbati, T. Berki, M. Morales, E. C. Azmitia, *Arch. Dermatol. Res.* **2006**, *298*, 99.
- [28] a) R. M. Z. Farahani, K. Sadr, J. S. Rad, M. Mesgari, *Adv. Skin & Wound Care* **2007**, *20*, 157; b) C. M. Nguyen, D. M. Tartar, M. D. Bagood, M. So, A. V. Nguyen, A. Gallegos, D. Fregoso, J. Serrano, D. Nguyen, D. Degovics, A. Adams, B. Harouni, J. J. Fuentes, M. G. Gareau, R. W. Crawford, A. M. Soulka, R. R. Isseroff, *Diabetes* **2019**, *68*, 1499.
- [29] D. J. Yoon, C. Nguyen, M. D. Bagood, D. R. Fregoso, H.-Y. Yang, A. I. Medina Lopez, R. W. Crawford, J. Tran, R. R. Isseroff, *J. Invest. Dermatol.* **2021**, *141*, 1608.
- [30] F. Su, H. Yi, L. Xu, Z. Zhang, *Neuroscience* **2015**, *294*, 60.
- [31] a) A. Salyani, C. Birt, *Canadian J. Ophthalmol.* **2005**, *40*, 170; b) A. Storm, E. Benfeldt, S. E. Andersen, J. Serup, *J. Am. Acad. Dermatol.* **2008**, *59*, 97; c) X. Tan, S. R. Feldman, J. Chang, R. Balkrishnan, *Expert Opin. Drug Deliv.* **2012**, *9*, 1263.
- [32] a) M. Koelch, A. K. Pfalzer, K. Kliegl, S. Rothenhöfer, A. G. Ludolph, J. M. Fegert, R. Burger, C. Mehler-Wex, J. Stingl, R. Taurines, K. Egberts, M. Gerlach, *Pharmacopsychiatry* **2012**, *45*, 72; b) I. Inkielewicz-Stepniak, *Pharmacological reports: PR* **2011**, *63*, 441; c) M. S. Golub, C. E. Hogrefe, *Psychopharmacology* **2014**, *231*, 4041.
- [33] N. Abdullayeva, M. Sankir, *Materials* **2017**, *10*, 586.
- [34] a) S. Chattopadhyay, L. B. C. Teixeira, L. L. Kiessling, J. F. McAnulty, R. T. Raines, *ACS Chem. Biol.* **2022**, *17*, 314; b) M. Dahlhoff, S. Muzumdar, M. Schäfer, M. R. Schneider, *The J. Investig. Dermatol.* **2017**, *137*, 921; c) R. Matsuo, M. Kishibe, K. Horiuchi, K. Kano, T. Tatsukawa, T. Hayasaka, M. Kabara, S. Inuma, R. Eguchi, S. Igawa, N. Hasebe, A. Ishida-Yamamoto, J.-I. Kawabe, *JID innovations: skin sci. mol. popul. health* **2022**, *2*, 100141; d) J. C. Zbinden, G. J. M. Mirhaidari, K. M. Blum, A. J. Musgrave, J. W. Reinhardt, C. K. Breuer, J. C. Barker, *Eur. Tissue Repair Society* **2022**, *30*, 82.
- [35] R. Mirza, T. J. Koh, *Cytokine* **2011**, *56*, 256.
- [36] D. Taverna, A. C. Pollins, G. Sindona, R. M. Caprioli, L. B. Nanney, *J. Proteome Res.* **2015**, *14*, 986.
- [37] K. Zlobina, E. Malekos, H. Chen, M. Gomez, *BMC Bioinformatics* **2023**, *24*, 166.
- [38] M. Jafari, G. Marquez, H. Dechiraju, M. Gomez, M. Rolandi, *Cell Rep. Physical Sci.* **2023**, *4*, 101535.
- [39] M. Jia, L. Luo, M. Rolandi, *Macromol. Rapid Commun.* **2022**, *43*, 2100687.
- [40] A. Gallegos, R. R. Isseroff, *MethodsX* **2022**, *9*, 101624.